Published in final edited form as:
J Am Chem Soc. 2012 August 1; 134(30): 12637–12647. doi:10.1021/ja303739g.

Modeling the Signatures of Hydrides in Metalloenzymes: ENDOR analysis of a di-iron Fe(μ-NH)(μ-H)Fe core

R. Adam Kinney[†], **Caroline T. Saouma**[‡], **Jonas C. Peters**[‡], and **Brian M. Hoffman**[†]

[†]Department of Chemistry, Northwestern University, 2145 Sheridan Road, Evanston, Illinois 60208, USA

[‡]Division of Chemistry and Chemical Engineering, California Institute of Technology, Pasadena, California 91125, USA

Abstract

The application of 35 GHz pulsed EPR and ENDOR spectroscopies has established that the biomimetic model complex $L_3Fe(\mu\text{-}NH)(\mu\text{-}H)FeL_3$ ($L_3 = [PhB(CH_2PPh_2)_3]^-$) complex, **3**, is a novel $S = ½$ type-III mixed-valence di-iron II/III species, in which the unpaired electron is shared equally between the two iron centers. $^{1,2}H$ and $^{14,15}N$ ENDOR measurements of the bridging imide are consistent with an allyl radical molecular orbital model for the two bridging ligands. Both the (μ-H) and the proton of the (μ-NH) of the crystallographically characterized **3** show the proposed signature of a 'bridging' hydride that is essentially equidistant between two 'anchor metal ions: a rhombic dipolar interaction tensor, $\mathbf{T} \approx [T, -T, 0]$. The point-dipole model for describing the anisotropic interaction of a bridging H as the sum of the point-dipole couplings to the 'anchor' metal ions reproduces this signature with high accuracy, as well as the axial tensor of a terminal hydride, $\mathbf{T} \approx [-T, -T, 2T]$, thus validating both the model and the signatures. This validation in turn lends strong support to the assignment, based on such a point-dipole analysis, that the molybdenum-iron cofactor of nitrogenase contains two [Fe-H^--Fe] bridging-hydride fragments in the catalytic intermediate that has accumulated four reducing equivalents (E_4). Analysis further reveals a complementary similarity between the isotropic hyperfine couplings for the bridging hydrides in **3** and E_4. This study provides a foundation for spectroscopic study of hydrides in a variety of reducing metalloenzymes in addition to nitrogenase.

Introduction

Both spectroscopic analysis and computational modeling of numerous metalloenzymes have implicated hydride intermediates within their active sites as relevant to catalysis. These include the Mo-dependent nitrogenase enzyme,[1] both the NiFe- and FeFe-hydrogenase enzymes,[2-4] CO-dehydrogenase,[5] and methyl co-enzyme M reductase.[6] As many of the studies implicating hydrido intermediates have relied on ENDOR spectroscopy, characterization of reference biomimetic complexes is an essential component to the study of these enzyme mechanisms. In addition, imide (NH^{2-}), is a proposed intermediate along the distal mechanism of N_2 reduction to NH_3,[7] and thus must be considered as a possible species formed during N_2 reduction by nitrogenase.[8,9] Therefore, study of this species in biomimetic complexes is likewise important.

Correspondence to: Jonas C. Peters; Brian M. Hoffman.

Supporting Information: Five ENDOR figures: ^2H ENDOR; ^1H PESTRE; ^1H and $^{14,15}N$ 2D field-frequency plots. This material is available free of charge via the Internet at http://pubs.acs.org.

Bridging hydrides have been invoked in a number of enzymatic settings. ^{1}H ENDOR responses measured from the $S = 1/2$ nitrogenase intermediate trapped during turnover of the V70I mutant nitrogenase enzyme under argon revealed the presence of two exchangeable protons with a distinct 'signature' that involves a highly anisotropic (rhombic) hyperfine coupling tensor. A point-dipole hyperfine coupling model was used to interpret this signature as being characteristic of metal-bridged hydrides,[1] and was subsequently used to assign the two protons as [Fe-H-Fe] fragments.[10] Step-annealing measurements of this intermediate identified it as the E_4 state of the enzyme, which has accumulated four electrons/protons and is primed for reaction with N_2.[11,12]

In the NiFe-hydrogenase enzymes, ^{1}H ENDOR has revealed the presence of a hyperfine-coupled hydrogenic ligand (A_{max} = -25 MHz), and DFT computations yielded hyperfine parameters consistent with the measured ENDOR response, thereby supporting a bridging geometry.[3] For FeFe-hydrogenase enzymes undergoing H^+ reduction or H_2 oxidation, transient metal hydrides, both terminal and bridging, have been modeled as possible intermediates in proposed reaction mechanisms.[4,13] In particular, the bridging geometry has been implicated in time resolved NMR and stopped-flow UV-vis measurements of model complexes,[14] and in a recent study wherein a ^{1}H isotropic hyperfine coupling, $|a_{iso}| = 76$ MHz, was measured by EPR spectroscopy, and supported by isotopic labeling and DFT calculations, for a proposed bridging hydride ligand in a delocalized Fe(I)-Fe(II) hydrogenase model complex.[15] However such hydrogenic ligands bound to the metal centers of the FeFe-hydrogenase enzyme have not been detected directly.

In contrast, an intermediate that was trapped for methyl-coenzyme M reductase showed a strongly-coupled ^{1}H ENDOR signal with an axial hyperfine tensor, which was assigned to a terminal hydride bound to Ni in a tetrapyrrole.[6] Recent studies of biomimetic, mononuclear Mo[16] and Fe complexes[17] have verified such an axial tensor as the signature of a terminal metal-hydride, but no equivalent study has been reported of a bridged hydride.

We here report the first ENDOR spectroscopic study of a crystallographically characterized model complex displaying a metal-bridged hydride in the form of an [Fe-H-Fe] fragment. Molecular hydrogen can be heterolytically split by reaction with $\{[PhBP_3]Fe)_2(\mu\text{-}N)\}^-$ ($PhBP_3 = PhB(CH_2PPh_2)_3^-$), **1**, a low-coordinate, low-spin di-iron II,II complex with a bridging nitride ligand (Scheme 1).[18] This reaction generates the unusual complex $\{\{[PhBP_3]Fe\}_2(\mu\text{-}H)(\mu\text{-}NH)\}^-$, **2**, containing two new bridging ligands, a hydride (H^-) and an imide (NH^{2-}). The ability to prepared appropriate isotopologues of **3** make it well suited for study by advanced paramagnetic resonance spectroscopies. ^{1,2}H and ^{14,15}N ENDOR measurements have yielded complete hyperfine tensors for all three atoms in the two bridging ligands, as well as the quadrupole tensor for the imido nitrogen. The experimental evaluation of the signs of the hyperfine couplings have aided in comparison to DFT calculations for both the anionic **2** and neutral, paramagnetic **3.** These studies unambiguously establish that this mixed-valence system exhibits a delocalized ground state. Analysis of the hyperfine couplings to the bridging hydride definitively confirm the point-dipole model for interpreting the hyperfine signatures of metal-bound hydrides, and in particular confirm the proposed signature of a bridging hydride, thereby confirming the assignment of the exchangeable hydrogenic ligands in the E_4 nitrogenase intermediate.

Materials and Methods

The isotopologues of $\{[PhBP_3]Fe\}_2(\mu\text{-}H)(\mu\text{-}NH)$ (**3**) ($[PhBP_3] = [PhB(CH_2PPh_2)_3]^-$) were synthesized according to published methods.[18] Briefly, a THF solution of $\{[PhBP_3]Fe\}_2(\mu\text{-}N)\{Na(THF)_5\}$ (**1**) was exposed to an atmosphere of H_2 to generate $\{[PhBP_3]Fe\}_2(\mu\text{-}H)(\mu\text{-}NH)\{Na(THF\}_5$ (**2**), which was subsequently oxidized to give $\{[PhBP_3]Fe\}_2(\mu\text{-}H)(\mu\text{-}NH)$

(**3**). The ^{15}N-enriched (50%) isotopologue, {[PhBP$_3$]Fe}$_2$(μ-H)(μ-$^{14/15}$NH), was prepared analogously from {[PhBP$_3$]Fe}$_2$(μ-$^{14/15}$N){Na(THF)$_5$}.[18] The fully deuterated isotopologue, {[PhBP$_3$]Fe}$_2$(μ-D)(μ-ND), was prepared by treatment of **1** with D_2 followed by oxidation. The mixed H/D isotopologue, {[PhBP$_3$]Fe}$_2$(μ-D)(μ-NH), was synthesized by stirring a THF solution of {[PhBP$_3$]Fe}$_2$(μ-H)(μ-NH){Na(THF)$_5$} under an atmosphere of D_2 for 2 h, followed by oxidation. {[PhBP$_3$]Fe}$_2$(μ-H)(μ-ND) was prepared analogously from {[PhBP$_3$]Fe}$_2$(μ-D)(μ-ND){Na(THF)$_5$} and H_2.

Crystals of **3** suitable for XRD were grown from the slow evaporation of pentanes into a saturated THF solution of **3**. The crystals were mounted on a glass fiber with Paratone N oil, and the data were collected on a Bruker SMART 1000 diffractometer with a CCD area detector under a stream of dinitrogen. The structure was determined using direct methods with standard Fourier techniques using the Bruker AXS software package[19,20] All non-hydrogen atoms were refined anisotropically. All hydrogen atoms (except the imido hydrogen and bridging hydride) were included in the model at geometrically calculated positions and refined using a riding model. The isotropic displacement parameters of all hydrogen atoms were fixed to 1.2 times the U value of the atoms they are linked to (1.5 times for methyl groups). The bridging hydride and imido hydrogen atom were located in the Fourier difference map, and the imido proton was refined semi-freely with the aid of distance restraints. One of the THF molecules was disordered, which was modeled as a two-component disorder. Similarity restraints on 1-2 and 1-3 distances, as well as similar ADP and rigid bond restraints, were applied to the disordered atoms.[21]

EPR/ENDOR samples of **3** were prepared in an N_2 filled dry-glove box. Briefly, THF, toluene, and 1:9 2-MeTHF:THF solutions of **3** (ca. 1-2 mM for all samples) were prepared from crystalline material and transferred to quartz capillaries. The samples were cooled in a cold well (pre-filled with liquid nitrogen), and the frozen solutions/glasses were immediately transferred to a dewar filled with liquid nitrogen.

35 GHz CW and pulse EPR and ENDOR spectroscopic data were collected on home-built spectrometers, described previously,[22-24] that were equipped with liquid helium immersion dewars for measurements at 2K. The CW measurements employed 100 kHz field modulation and dispersion mode detection under rapid passage conditions. ^{1}H CW ENDOR spectra employed broadening of the RF to 100 kHz to improve signal-to-noise.[25] ^{1}H CW ENDOR spectra were collected using the stochastic-field modulation detected ENDOR sequence,[26] to improve ENDOR lineshapes. Data acquisition for all pulse experiments utilized the SpecMan software package (http://specman.4epr.com) in conjunction with a Spin-Core PulseBlaster ESR_PRO 400 MHz word generator and an Agilent Technologies Acquiris DP235 500MS/sec digitizer.

For a single molecular orientation and for nuclei with nuclear spin of I = ½ (^{1}H, ^{15}N, ^{31}P), the ENDOR transitions for the $m_s = \pm½$ electron manifolds are observed, to first order, at frequencies,

$$\nu_{\pm} = |\nu_n \pm A/2|$$

where ν_n is the nuclear Larmor frequency, and A is the orientation-dependent hyperfine coupling. For I ≥1 (^{2}H, ^{14}N, I = 1; ^{11}B, I = 3/2), the two ENDOR lines are further split by the orientation-dependent nuclear quadrupole coupling (P). The frequency for the $m_I \leftrightarrow (m_I - 1)$ ENDOR transition is then given by

$$\nu_{\pm,m_I} = \left|\nu_{\pm} \pm (3P/2)(2m_I - 1)\right|$$

In the Mims experiment, the ENDOR intensities are modulated by the response factor (R) inherent to the experiment, which is a function of the product of the hyperfine coupling (A) and the time between the second and third microwave pulses in the three-pulse sequence (τ), and given by the equation,

$$R \sim [1 \cos(2\pi A\tau)]$$

When $A\tau = n$ ($n = 0,1,2,\ldots$), the ENDOR response is at a minimum, resulting in hyperfine 'suppression holes' in the Mims spectra.

At the low and high field edges of the EPR spectrum (g_1 and g_3, respectively), ENDOR interrogates only a single molecular orientation ('single-crystal-like' position). At intermediate fields, however, ENDOR interrogates a well-defined subset of molecular orientations. By analyzing a 2D field-frequency ('orientation-selective') pattern of ENDOR spectra taken at numerous fields across the EPR envelope, it is generally possible to determine the complete hyperfine and quadrupole tensor principal values and their orientations relative to **g**.[27,28] The uncertainties in the reported hyperfine and quadrupole couplings are estimated to be no greater than ~5%, unless otherwise stated.

Signs of the hyperfine couplings measured from ENDOR spectra (more specifically, the sign of $g_{Nuc}A_{Nuc}$) have been obtained by application of the Pulse-Endor-SaTuration-Recovery (PESTRE) protocol,[29] a pulse sequence comprised of multiple Davies ENDOR sequences, carried out in three distinct experimental phases: (I) an EPR saturation phase (RF off) of 100 Davies sequences whose spin-echo intensities quickly converge to the steady-state 'baseline' (BSL); (II) an ENDOR perturbation phase of 24 sequences, in which each sequence contains a fixed RF set at one or the other of the branches of the ENDOR spectrum ($\nu_{\pm}$); (III) and an EPR recovery phase (RF off) of 132 sequences during which the spin echo corresponds to the spin-echo 'dynamic reference level' (*drl*) associated with ENDOR-induced spin polarization created in the second phase, with the *drl* relaxing to the BSL during this phase. In the slow-relaxation regime, the sign of A_{Nuc} is unambiguously given by the sign of the difference between the *drl* and BSL echo intensities as observed for *either* ENDOR branch.

Density functional theory calculations were carried out using the Amsterdam Density Functional (ADF) software suite.[30] Geometry optimization of **2** and **3** was performed on the complete molecule using the BLYP density functional and a TZP basis set with a small frozen core potential to reduce computation time. For the paramagnetic **3**, all calculations were performed in the spin unrestricted formalism with a spin polarization of 1 ($S = 1/2$). Single point calculations utilized the all electron TZ2P basis with an integration factor of 4.

Results

Synthesis and characterization of 3

The mixed-valence imide-hydride **3** is readily prepared in two steps from the di-ferrous bridging nitride anion, $\{\{[PhBP_3]Fe\}_2(\mu\text{-}N)\}\{Na(THF)_5\}$ (**1**) (Scheme 1). As previously reported,[18] exposure of a THF solution of **1** to an atmosphere of H_2 generates the di-ferrous imide hydride, $\{\{[PhBP_3]Fe\}_2(\mu\text{-}NH)(\mu\text{-}H)\}\{Na(THF)_5\}$ (**2**), and subsequent oxidation of **2** with one equivalent of $(NO)(BF_4)$ or PCl_3 generates mixed-valence $\{[PhBP_3]Fe\}_2(\mu\text{-}H)(\mu\text{-}NH)$, **3**. Though solutions of **2** are stable to H_2, the bridging hydride and μ-N*H* hydrogen

atoms selectively exchange when exposed to D_2 over the course of hours and days, respectively. Thus, stirring a THF solution of the parent **2** under a D_2 atmosphere for two hours results in complete deuterium substitution at the bridging hydride ligand and formation of $\{[PhBP_3]Fe\}_2(\mu\text{-}D)(\mu\text{-}NH)$, as is evident from the loss of the hydride signal in the ^1H NMR spectrum of mono-deuterated **2**. The imido μ-N*H* resonance is retained in the ^1H NMR spectrum. Incubating **2** for days additionally washes out the μ-N*H* resonance to give di-deuterated $\{\{[PhBP_3]Fe\}_2(\mu\text{-}D)(\mu\text{-}ND)\}\{Na(THF)_5\}$, **2**. These deuterated precursors thereby afford access to the analogous labeled complexes of **3** by the aforementioned oxidation protocol.

The solid-state structure of mixed-valence **3** is shown in Fig. 1. The dataset was of sufficient quality to allow both the hydrido and imido protons to be located in the Fourier difference map. The metrical parameters about the iron centers are summarized in Table 1, and are compared to those previously reported for di-ferrous **2**.[18] Upon oxidation, the average Fe-N distance decreases by *ca.* 0.3 Å to 1.78 Å, and the average Fe-P bond distance increases by *ca.* 0.07 Å. This trend has also been observed in the related low-spin (S = 0) imido species, $[PhBP_3]Fe{\equiv}N(1\text{-Adamantyl})^{-/0}$, and has been attributed to increased Fe-P π backbonding in the reduced congener.[31] The metrical parameters for both iron ions of **3** (S = ½) are similar, suggesting delocalization of the unpaired electron.

EPR Characterization of 3

The 35 GHz EPR spectrum of **3** (Fig. 2) exhibits a near-axial EPR spectrum, with a small rhombic splitting, that also is manifest in ^1H ENDOR measurements (see below): **g** = [2.54, 2.047, 2.031]. As described below, ^1H and ^{11}B ENDOR measurements assign the unique magnetic direction (g_1) to lie along the Fe-Fe vector, with g_2 normal to the plane defined by the Fe(μ-H)(μ-NH)Fe core and g_3 (approximately) collinear with the NH-H vector.

The perpendicular region of the 10 K X-band EPR spectrum of **3** shows partially resolved hyperfine structure that can be simulated with a single strongly coupled proton (see below) and six equivalent ^{31}P nuclei each having $A_\perp$ = 12 G (not shown).[18] This analysis indicates that the electron spin is symmetrically delocalized. Although the ^{31}P couplings are not resolved at higher temperatures or in the 35 GHz EPR spectrum of **3**, the g values in the spectra at the two frequencies are invariant from 77 K to 2 K, indicating that the spin does not localize at low temperature, and that **3** is ideally described as a type-III delocalized mixed valence complex.[32]

$^{1,2}H$ ENDOR of 3

The ^1H stochastic-field modulation-detected (stochastic CW) ENDOR spectrum of **3** at g_2 (Fig. 3) shows two well-resolved ^1H ENDOR signals, with one appearing over a range of frequencies around the hyperfine coupling A ≈ 56 MHz, $\Delta\nu_+$ = 25 MHz, and one a sharp signal corresponding to A ≈ 12 MHz. Selective deuterium labeling of the bridging ligands (see above) generated the four $^1H/^2H$ isotopomers of **3** ($^1H_{NH}/^1H_\mu$; $^1H_{NH}/^2H_\mu$; $^2H_{NH}/^1H_\mu$; $^2H_{NH}/^2H_\mu$). Their ENDOR responses at g_2 identify the ENDOR signals with the larger coupling as corresponding to the bridging hydride ($^1H_\mu$), and the signal with the smaller coupling as from the proton of the bridgingimido ligand ($^1H_{NH}$) (Fig. 3).

Bridging Hydride—The 2D field-frequency pattern of stochastic CW ^1H ENDOR spectra for the bridging hydride is shown in Fig. 4. The large $^1H_\mu$ hyperfine coupling ($|A_{max}|$ = 56 MHz) leads to a substantial overlap between ν_- of the $^1H_\mu$ ENDOR response and ν_+ of the ^{31}P ENDOR response across the entire EPR envelope. At all fields, the $^1H_\mu$ ν_+ ENDOR response, however, is isolated from all other ENDOR responses, permitting analysis of

the $^{1}H_{\mu}$ hyperfine tensor. In the $^{1,2}H_{NH}/^{2}H_{\mu}$ isotopologues, the $^{1}H_{\mu}$ signal is lost and replaced by a $^{2}H_{\mu}$ signal with the corresponding hyperfine coupling, $|A(^{2}H)_{max}| = 8.6$ MHz.

To extract the full hyperfine tensor and its orientation relative to **g**, ^{1}H ENDOR spectra were obtained at multiple field positions across the EPR envelope (Fig. 4).[28,33] Excellent simulation of the 2D field-frequency pattern was achieved with a hyperfine tensor for $^{1}H_{\mu}$ of $\mathbf{A} = -[19.5, 56.3, 41.0]$ MHz $= a_{iso}\mathbf{1} + \mathbf{T}$, where $a_{iso} = -38.9$ MHz, and the through-space electron-nuclear dipolar interaction between the bridging hydride and the unpaired spin on the iron nuclei is $\mathbf{T} = [+19.4, -17.4, -2]$ MHz, nearly coaxial with **g**. The optimal simulation employs a small rotation of **A, T** around the $g_2(y)$ axis ($\beta = 5°$), which tilts the A_3, T_3 principal axis slightly out of the g_2-g_3 plane.

The relative signs of the tensor components are determined by the simulations; absolute signs were determined through application of the PESTRE technique to the $\nu_{\pm}$ $^{2}H_{\mu}$ ENDOR features at g_2 (not shown).[29] This result agrees with the expectation that $T_{max} > 0$ (for $g_n > 0$) because it is dominated by through-space electron-nuclear dipolar interactions. The result, $a_{iso} < 0$, indicates that the spin on the bridging hydride results from spin polarization of the filled (d_{π}-σ(H)) bonding orbitals.

Dipolar Coupling and the g Tensor Orientation—By orienting the components of the through-space electron-nuclear dipolar coupling tensor for H_{μ}, **T**, in the molecular frame, we can directly determine the orientation of **g** in that frame. When g anisotropy is small, the through-space dipolar component of the hyperfine coupling, **T**, can be well described by an approximate expression for a binuclear center, eq 1,

$$\widehat{H}_{DD} \approx \overline{g}_e g_n \beta_e \beta_n \sum_i \widehat{S}_i^T \cdot T_i \cdot \widehat{I} \qquad (1)$$

where **T** has the well-known form of a traceless ($T_1 + T_2 + T_3 = 0$) symmetric tensor. As such, it lends itself well to the determination of the metrical parameters that relate the position of nuclei being examined to the g tensor, and ultimately to the molecular frame.[34,35] However, when g anisotropy is substantial, as in the present study, the general form of this interaction must be employed, eq 2,

$$\widehat{H}_{DD} = g_n \beta_n \sum_i \widehat{\mu}_i \cdot T_i \cdot \widehat{I} \qquad (2)$$

which employs the orientation dependent magnetic moment, $\hat{\boldsymbol{\mu}}_i = \beta_e \mathbf{B_0}\,[\hat{\boldsymbol{S}} \cdot \mathbf{g} \cdot \boldsymbol{b}]$ in the presence of an external field, $\mathbf{B_0} = B_0\mathbf{b}$.[36] This leads to a non-symmetric dipolar coupling matrix that does not lend itself to a simple determination of its orientation within the molecular frame through coordinate transformations based on rotation matrices and Euler angles.[34,35] To carry out the analysis of the ENDOR data obtained for **3** we have combined the approach of Hutchison and McKay for the treatment of an anisotropic magnetic moment[36] into a treatment that describes the dipolar interaction of a nucleus with a paramagnetic di-metal center.[37] We find that simplifications introduced by symmetry at the bridging hydride and NH moieties of **3** lead to the resultant, symmetric dipole interaction of the form of eq 1.

We begin by defining a convenient molecular coordinate frame. Given that the Fe(μ-H)Fe moiety is nearly mirror symmetric relative to the plane bisecting the FeHFe angle, normal to the FeHFe plane, we take z to be along the FeFe vector, and x to lie in that plane normal to the FeFe vector (Fig. 5), and y to be normal to the Fe(μ-H)Fe plane. In this frame the orientation of the applied magnetic field is described by directional cosines for Fe_1H and Fe_2H, eq 3:

$$\begin{pmatrix} l_x^{A/B} & l_y^{A/B} & l_z^{A/B} \end{pmatrix} = \begin{pmatrix} \sin\theta & 0 & \pm\cos\theta \end{pmatrix} \quad (3)$$

The crystal structure of **3** gives Fe-H bond lengths of 1.64(3) and 1.68(3) Å, and equivalent Fe-Fe-H angles of 40(1)°. To simplify, we symmetrize the structure by setting r(Fe_1-H) = r(Fe_2-H) = r = 1.66 Å. The resulting, nonsymmetric, point-dipole interaction matrices for a spin on $Fe_{1/2}$ are given by eq. 4,

$$\mathbf{T}^{1/2} = T_{nl} \begin{pmatrix} g_x/g_e & 0 & 0 \\ 0 & g_y/g_e & 0 \\ 0 & 0 & g_z/g_e \end{pmatrix} \begin{pmatrix} 3\sin^2\theta - 1 & 0 & \pm 3\sin\theta\cos\theta \\ 0 & -1 & 0 \\ \pm 3\sin\theta\cos\theta & 0 & 3\cos^2\theta - 1 \end{pmatrix}, \quad T_{nl} = \frac{g_e \beta_e g_n \beta_n}{r^3} \quad (4)$$

The complete dipolar hyperfine tensor for the hydride of a $S = ½$ spin-coupled/spin-delocalized center, $\mathbf{T_d}$, is obtained by addition of the dipolar couplings to the two Fe ions, $\mathbf{T}^1$ and $\mathbf{T}^2$, scaled by the spin-projection coefficients/spin-densities at each iron, $K_{A/B}$,

$$T_d = K_1 T^1 + K_2 T^2 \quad (5a)$$

For $K_1 \neq K_2$ and/or a nucleus at a general location in the molecular frame, $\mathbf{T_d}$ also is non-symmetric, with the disadvantages noted above. However, for nuclei equidistant from Fe_1 and Fe_2, such as is the case for the μ-H and μ-NH moieties, *and* with $K_1 = K_2 = K$, the dipolar tensor reduces to a simple, diagonal form proportional to K. Complex **3** has a single spin equally delocalized between the two Fe ions, as initially inferred from the ^{31}P hyperfine couplings (and see below), giving $K_1 = K_2 = K = ½$, which leads to the symmetric (diagonal) form, eq. 5b,

$$T_d = \frac{T_{nl}}{2} \begin{pmatrix} \left(g_x/g_e\right)(3\sin^2\theta - 1) & 0 & 0 \\ 0 & -\left(g_y/g_e\right) & 0 \\ 0 & 0 & \left(g_z/g_e\right)(3\cos^2\theta - 1) \end{pmatrix} \quad (5b)$$

This can further be decomposed into the sum of an isotropic (pseudo-contact) term, a'_{iso}, and a diagonal, traceless dipolar matrix, $\mathbf{T'}$, of the form of eq 1, eqs. 6a-6d,

$$\mathbf{T_d} = a'_{iso}\mathbf{1} + \mathbf{T'} \quad (6a)$$

where

$$a'_{iso} = \frac{Tr(T)}{3} = \frac{T_{nl}}{3}\left(\left(\frac{g_x}{g_e}\right)(3\sin^2\theta - 1) - \left(\frac{g_y}{g_e}\right) + \left(\frac{g_z}{g_e}\right)(3\cos^2\theta - 1)\right) \quad (6b)$$

and $\mathbf{T'}$ has principal components,

$$\begin{aligned} T'_{xx} &= -\tfrac{T_{nl}}{3}\left[-2\left(g_x/g_e\right)(3\sin^2\theta - 1) - \left(g_y/g_e\right) + \left(g_z/g_e\right)(3\cos^2\theta - 1)\right] \\ T'_{yy} &= -\tfrac{T_{nl}}{3}\left[\left(g_x/g_e\right)(3\sin^2\theta - 1) + 2\left(g_y/g_e\right) + \left(g_z/g_e\right)(3\cos^2\theta - 1)\right] \\ T'_{zz} &= -\tfrac{T_{nl}}{3}\left[\left(g_x/g_e\right)(3\sin^2\theta - 1) - \left(g_y/g_e\right) - 2\left(g_z/g_e\right)(3\cos^2\theta - 1)\right] \end{aligned} \quad (6c)$$

As a result, a 2D field-frequency pattern of $^{1}H_{\mu}$ ENDOR spectra can be analyzed interms of the standard form of the hyperfine coupling tensor, **A**,

$$\mathbf{A}=a_{iso}(obs)\mathbf{1}+\mathbf{T}'$$
$$a_{iso}(obs)=a_{iso}+a'_{iso}, \quad (6d)$$

where a_{iso} is the true isotropic coupling due to s-orbital spin density, Analysis of a 2D ENDOR pattern yields the diagonal components of $\mathbf{T}'$ and the orientation of this interaction relative to the **g** and molecular frames, as described by the Euler angles that relate these frames. The distance of the nucleus under examination from the Fe ions is given by $\mathbf{T_{nl}}$ (eq 4b).

Simulation of the 2D field-frequency ENDOR pattern of the bridging hydride shows that **g** and **A** are essentially coaxial (±5°), with corresponding observed dipole tensor components, $\mathbf{T} = [T_1, T_2, T_3] = [19.4, -17.4, -2.0]$ MHz, closely approximating to a fully rhombic interaction, $\mathbf{T} \sim [T, -T, 0]$. Such a signature tensor is predicted by eq. 6c for the bridging hydride, with the unique, T_{xx}', component lying in the Fe-H-Fe plane, along the bisector of that angle. Detailed comparisons with the structurally determined tensor components of the traceless dipolar interaction of eq. 6c, $\mathbf{T}'$, as calculated for all possible relative assignments of the g_i and T'_{jj} then establishes that the measured **T** corresponds to the calculated $\mathbf{T}'$ for an assignment in which the unique g-value, $g_1 = 2.54$, lies along the Fe-Fe vector; $g_2 = 2.047$, is perpendicular to the Fe-H-Fe plane (and thus the Fe-(NH)-Fe plane),; and g_3 lies in the Fe-H-Fe plane, normal to the Fe-Fe vector (along the Fe-H-Fe bisector). The result of this analysis is visualized in Fig. 5. ENDOR measurements on the ^{11}B and ^{31}P nuclei of **3** (Fig. 6), discussed below, likewise indicate that g_1 corresponds to g_z. The tensor components of $\mathbf{T}'$ computed from eq. 6c and the symmetrized metrical parameters obtained from the crystal structure, without adjustment of the structure or modifications of the K_i from spin delocalization, are in excellent agreement with **T** obtained from experiment: $\mathbf{T}' = [T'_{zz}, T'_{yy}, T'_{xx}] = [16.4, -19.0, 2.57]$ MHz.[38] The computed rhombic tensor of an $[M_1\text{-H-}M_2]$ fragment smoothly evolves into the signature axial tensor, $\mathbf{T} \approx [T, -T, 2T]$ for a terminal hydride as the proton is moved to one side of the $[M_1, M_2]$ unit.

Imido Proton: The proton of the bridging imido ligand exhibits a maximum ^{1}H hyperfine coupling of 12 MHz at g_2 (Fig. 3). A complete analysis of the 2D field-frequency ^{1}H pattern was precluded by the overlap of the ENDOR patterns from the imido proton and the weakly coupled protons of the tris(phosphino) borate ligand and the solvent matrix. Instead, we analyzed the ^{2}H Mims 2D field-frequency ENDOR pattern acquired from the fully deuterated isotopologue of **3**, Fig. 7. Although this pattern is exceptionally well-resolved and complex, the spectra measured at the three principal g values are fully resolved so that the hyperfine couplings and ^{2}H quadrupole splitting can be read off directly. With these couplings as initial estimates of the tensor principal values, the hyperfine and quadrupole tensors have been refined so as to reproduce the full 2D pattern.

To begin, the magnitudes of the ^{2}H hyperfine coupling tensor principal values were approximated from the Mims ENDOR spectra taken at g_1, g_2, and g_3: $|A_1| = 0.5$ MHz, $|A_2| = 1.4$ MHz, and $|A_3| = 0.5$ MHz, respectively. Given the Fe-H_{NH} distance of approximately 2.50 Å, the contribution to the A_i from the through-space dipolar coupling is expected to be comparable with a_{iso}. Simulation of the ENDOR pattern then requires that we discriminate among the four possible hyperfine tensors that differ with respect to the *relative* signs of the principal values: $A^{i} = \pm[0.5, 1.4, -0.5]$; $A^{ii} = \pm[0.5, -1.4, 0.5]$; $A^{iii} = \pm[-0.5, 1.4, 0.5]$; and $A^{iv} = \pm[0.5, 1.4, 0.5]$ MHz. This was achieved by taking advantage of the hyperfine suppression effect inherent to the Mims ENDOR experiment. In an ENDOR pattern in which the signs of the hyperfine principal values are not all the same, the ν_+ and ν_- ENDOR responses must

cross through $\delta\nu = \nu - \nu_n(^2H) = 0$ MHz ($A_{obs} = 0$ MHz), thus yielding an ENDOR response in the vicinity of $\delta\nu = 0$ MHz. In a Mims experiment, this response is suppressed (the $n = 0$ suppression hole; see above), but the suppression effect diminishes as the interval between the first and second pulses in a Mims experiment, τ, is increased. This allows discrimination among the different tensors by comparing spectra collected over a range of τ values with the corresponding Mims ENDOR simulations for the three tensor options.

This technique was applied to ENDOR spectra taken with multiple τ at magnetic fields corresponding to g = 2.038, 2.046, 2.20, and 2.33. Simulations at g = 2.20 and 2.33 are dominated by A_2 and A_3, and involve orientations in which the magnetic field lies in the g_1-g_2 plane where the isotropic and dipolar coupling cancel. These simulations exhibit a peak centered at $\nu \sim \nu_n(^2H)$. If such a feature existed, it would be enhanced at $\tau = 800$, compared to $\tau = 500$ ns. However, spectra collected at these two intervals show no difference in the Mims ENDOR response (Fig. S1A, B), effectively ruling out A^{ii} and A^{iii}. The remaining two tensors, A^i and A^{iv}, are ideally tested at a field between g_2 and g_3. Simulations for A^{iv} generate no ENDOR response at $\delta\nu = 0$ MHz, in contrast with the A^i simulations, which correctly predict the ENDOR response at $\delta\nu = 0$ MHz that is observed in the spectra at g = 2.038 and 2.046 (Fig. S1C, D). The hyperfine tensor for the imido deuteron is therefore $\mathbf{A}(^2H) = \pm[0.5, 1.4, -0.5]$ MHz, with **A** oriented relative to **g** by ±10° from the Fe(μ-NH)Fe plane. Although the ^1H ENDOR pattern could not itself be analyzed, the corresponding ^1H ENDOR pattern obtained by scaling $\mathbf{A}(^2H)$ by the ratio of the proton and deuteron nuclear g values ($g_n(^1H)/g_n(^2H) = 6.51$) reproduce well the outer edge of the ^1H ENDOR pattern (Fig. S2).

The absolute sign of the isotropic hyperfine coupling to the imido proton was determined by application of the PESTRE technique, Fig. S3. Under 'standard' conditions, in which the time between the second and third Davies microwave pulses is short relative to the electron spin-lattice relaxation time ($t_{mix} \ll T_{1e}$), the PESTRE responses measured at g_2 for both ν_+ and ν_- are weak, but can be assigned as α and β transitions, respectively. This assignment was confirmed by the technique of variable mixing time (VMT) Davies ENDOR,[39,40] wherein t_{mix} is increased such that $T_{1e} \sim t_{mix}$ (see SI)

These findings show that $a_{iso}(^1H_{NH}) < 0$, implying negative spin density on the proton, $\rho_H < 0$,[16,29] and a hyperfine tensor, $\mathbf{A}(^2H_{NH}) = -[0.5, 1.4, -0.5]$ MHz, $a_{iso}(^2H_{NH}) = -0.47$ MHz, and **T** = [-0.03, -0.93, 0.97] MHz. The anisotropic coupling of the imido deuteron is, like that of the bridging hydride, fully rhombic. $\mathbf{T}(^2H_{NH}) \sim [0, -1, +1]$ MHz. This is in full agreement, with the coupling calculated for the [Fe-(NH)-Fe] fragment through the point-dipole anisotropic interaction with the delocalized spin on the two Fe ions (eq 6c): $\mathbf{T'}(^2H_{NH}) = [-0.2, -0.8, 1]$ MHz (corresponding to $\mathbf{T}'(^1H_{NH}) = [-1.3, -5.2, 6.5]$ MHz). We further find from that ~3 % of the measured a_{iso} is associated with the pseudo-contact contribution (eq. 6b, a_{iso}')

The ^2H quadrupole splitting is fully resolved in the ENDOR spectra measured at each of the principal g values (Fig. 7) and was refined by simulation of the complete pattern, leading to a ^2H quadrupole coupling tensor, $\mathbf{P} = \pm[0.06, 0.06, -0.12]$ MHz, coaxial with **A** (and **g**) within the resolution of the experiment ($\beta \sim \pm 5°$). For comparison with other formulations of the quadrupole interaction, we note that $P_{max}/2 = e^2qQ/4h = K(^2H) = \pm 0.24$ MHz (the symbols having their usual definitions).

^{11}B and ^{31}P ENDOR

A ^{11}B Mims ENDOR 2D field-frequency pattern is presented in Fig. 6 (*left*). The spectrum at g_1 shows a hyperfine-split doublet centered at ν_B, with each partner showing an

additional triplet splitting caused by the nuclear quadrupole interaction ($I(^{11}B)=3/2$). As shown, the 2D pattern can be simulated using a single hyperfine tensor and single quadrupole tensor. This analysis in terms of a single type of ^{11}B nucleus confirms that the ^{11}B nuclei of the two $PhBP_3$ ligands are magnetically and geometrically equivalent, as expected from the near mirror symmetry of the molecule (see Scheme 1) and the symmetrical delocalization of the electron spin of **3** (see below). In keeping with the molecular symmetry, the two tensors have nearly axial symmetry, with the unique direction lying along the B-Ph bond, corresponding to g_1, and are essentially coaxial with the FeFe bond as described above. The principal values of the tensors are: $\mathbf{A}(^{11}B)$ = [0.68(02), -0.40(05), -0.50(03)] MHz, a_{iso} = -0.07 MHz, $\mathbf{T}(^{11}B)$ ~ [0.75, -0.33, -0.43] MHz, where the signs of the principal values are assigned such that $T_{max} > 0$. The vanishingly small value of a_{iso} implies that there is negligible spin density on boron (< 0.1% of a spin per B), as expected given the absence of a direct B-Fe bonding interaction. The quadrupole tensor components are, $\mathbf{P}(^{11}B)$ = ±[-0.042, 0.018, 0.024] MHz, with the small coupling (K = ±0.021 MHz, $\eta = 0.14$) again as expected for the nearly tetrahedral symmetry at boron.

The six P-atoms from the two $PhBP_3^-$ ligands coordinating the two Fe ions show a single ν_+ ENDOR response in *sf*-ENDOR measurements (Fig. 6, *right*), as expected for six magnetically equivalent ^{31}P nuclei interacting with a symmetrically delocalized electron spin. The 2D ^{31}P ENDOR pattern reveals that the ^{31}P hyperfine coupling is primarily isotropic, a_{iso} ~ ±36 MHz. As a single electron in the 3s orbital of phosphorous would give a hyperfine coupling of ~1.3×10^4 MHz,[41] this indicates that spin density is delocalized into the 3s orbital of each phosphorous to a minimal extent, ~0.3%; taking the bonding orbital to have sp^3 hybridization, only ~ 1% of the spin is delocalized onto each of the six phosphorous ligands.

^{14,15}N ENDOR

Davies $^{14/15}$N ENDOR spectra of the 50% ^{15}N labeled isotopologue of **3** are presented in Fig. 8. The spectrum measured at $g_3 = 2.031$ shows ^{14}N and ^{15}N Larmor-centered ENDOR doublets corresponding to $A_3(^{14}N) = 2.52$ MHz and $A_3(^{15}N) = 3.54$ MHz, appropriately related by the ratio of the nuclear g-values, with the two branches of the former further showing a quadrupole splitting, $3|P| = 0.36$ MHz. The $^{14/15}$N hyperfine coupling measured at g_3 is the minimum observed at any field. The maximum hyperfine coupling is observed at g_2, $A_2(^{14/15}N) = 5.7/8.0$ MHz. The ^{14}N ENDOR response at g_1 is not satisfactorily resolved in a Davies ENDOR experiment, but was measurable in a 35 GHZ CW ENDOR spectrum (Fig. 8), $A_1(^{14/15}N) = 3.0/4.1$ MHz. The anisotropy in the magnitudes of the hyperfine coupling is noticeably larger than usually observed for a nitrogenous ligand σ-bonded to Fe (e.g. histidine),[42,43] which indicates that the unpaired spin at the $^{14/15}$N ligand in fact is associated with an orbital having significant π-character.

The signs of the ^{14}N hyperfine tensor elements were evaluated with the VMT-ENDOR experiment (Fig. 9). Normalization of the Davies ENDOR spectra acquired with t_{mix} values of 5, 1000, and 3000 μs to the ^{14}N ν_- ENDOR response shows that the ν_+ ENDOR response is decreasing as the mixing time is increasing. Such behavior is characteristic of an ENDOR response that originates from the α electron spin manifold ($m_s = -1/2$), which indicates that $\mathbf{A}(^{14}N) < 0$. The sign of the third tensor component, A_1, was determined from simulations of the 2D ^{15}N field-frequency ENDOR pattern (see below). The ^{15}N ENDOR spectra measured at the principal g values can be well simulated using the hyperfine couplings listed above and *coaxial* **g, A**, and **P** (Fig. 8).

A simulation of the ^{15}N 2D field-frequency ENDOR pattern (g = 2.031 to 2.190) generated from the parameters presented above, with $A_1 < 0$, and with the dipolar tensor slightly

rotated relative to **g** around the out-of-plane g_2 (y) axis ($\beta \leq 5°$), matches the behavior of the data fairly well, notably along the high frequency edge corresponding to the A_2, $\nu_+(^{15}N)$ ENDOR response, Fig. S4 (A_3,$\nu_-(^{15}N)$ overlaps A_2,$\nu_+(^{14}N)$ and is not resolved). In contrast the pattern generated with $A_1 > 0$ does not match well. The results then yield as the hyperfine tensors for ^{14}N and ^{15}N, $\mathbf{A}(^{14}N)$ = -[3, 5.7, 2.5] MHz, and $\mathbf{A}(^{15}N)$ = +[4.1, 8, 3.5] MHz.

The ^{14}N tensor can be decomposed into an isotropic term, a_{iso} = -3.7 MHz, and anisotropic term, **T** ~ -[-0.75, +2.0, -1.25] MHz, with the largest tensor component (T_2 = 2.0 MHz) lying along g_2, normal to the Fe-NH-Fe plane (see above). This tensor in turn can be decomposed into two orthogonal axial tensors, a major contribution $\mathbf{T_2}$ = -[-1.1, 2.2, -1.1] MHz, with its unique axis along g_2, and a minor one, $\mathbf{T_1}$ = -[0.3, -0.15, -0.15] MHz, with its unique value along the FeFe axis (g_1, z).

The isotropic coupling is very small compared to that expected for one electron in a ^{14}N 2s orbital, a_{iso}^0 = 1810 MHz, corresponding to a 2s spin density of $\rho_s \sim 2\times10^{-3}$.[41] It can also be shown that the tensor $\mathbf{T_2}$ is proportional to the difference between the spin density in the 2pπ orbital normal to the Fe-NH-Fe plane and the average of the spin densities in the 2pσ orbitals. Given the small isotropic coupling and trigonal geometry at N, this anisotropic contribution is clearly dominated by spin density in the 2pπ orbital. Given the unique value for the anisotropic coupling to a single electron in a ^{14}N 2p orbital is $2T^0$ = 110 MHz,[41] the 2pπ spin density is therefore ~ -0.02.

The ^{14}N quadrupole splitting is well resolved in the Davies spectra collected at g_2 and g_3 and only partially resolved in the spectrum at g_1 due to overlap with the ^{15}N ν_- ENDOR response. However, the quadrupole splitting is resolved for the ν_+ ENDOR response from the CW spectrum measured at g_1. As the quadrupole tensor must be traceless, the measured splittings lead to the quadrupole tensor, **P** = +[0.19, -0.31, 0.12], where the absolute sign of the nuclear quadrupole coupling constant is assigned from the known sign of the quadrupole moment.[44] ^{14}N simulations generated with the above **P** match the Davies ENDOR spectra measured at g_2, g_3, and both the Davies and CW spectra measured at g_1 (Fig. 8). The quadrupole tensor is roughly axial, η = 0.23, compared to the maximum value, η = 1, with the unique axis lying along the p-π orbital normal to the Fe-NH-Fe plane, as expected for a 'trigonal-planar'imide.

The partial 2D pattern of ^{14}N ENDOR spectra shown in Fig. S5 (g = 2.031 to 2.152) can be adequately represented by the spin Hamiltonian with $\mathbf{A}(^{14}N)$ and $\mathbf{P}(^{14}N)$ given above, with a slight rotation of the tensors around the out of plane g_2 (y) axis ($\beta \leq 5°$) relative to **g**. The near coaxiality of the three tensors is sensible considering the near two-fold rotational symmetry of the bridging imido (and hydrido) ligand (Scheme 1).

Discussion

We have carried out a comprehensive EPR and ENDOR spectroscopic study of the crystallographically characterized mixed-valence bridging imide/hydride (**3**) that displays one structural element involved in nitrogen fixation by nitrogenase and a second that might be: (i) [Fe-H-Fe], and (ii) [Fe-NH-Fe]. Below, we first discuss how the EPR and ENDOR results characterize the ground state of **3** as a type-III mixed-valence di-iron complex, comparing the present report with DFT calculations of **3** and the one-electron reduced congener, **2**. We next compare dipole interaction matrix, **T'**$_s$obtained through analysis of the proton ENDOR measurements of the [Fe-H-Fe] moiety of **3** with the matrix computed from the structure through use of a simple point-dipole model for a hydride bridging two metal ions[37] as refined above. The comparison validates our use of this model for **3**, and therefore

its use to assign as [Fe-H-Fe] bridging hydrides the two magnetically equivalent ^{1}H nuclei bound to FeMo-co in the E_4 intermediate trapped during turnover of the V70I nitrogenase mutant under Ar.[1]

Delocalization of the Electronic Ground State of 3

The EPR spectrum of **3** is characterized by a strongly anisotropic g tensor, **g** = [2.54, 2.047, 2.031], in keeping with what might be expected for a low-spin d^5 ion in a geometry describable as being distorted from trigonal.[45,46] In the 4K EPR spectrum of **3**, hyperfine coupling to the hydride and the phosphorous nuclei are partially resolved (see SI).[18] The hyperfine pattern can be simulated with a single strongly coupled ^{1}H nucleus ($^{1}H_{\mu}$) and six 'equivalent', more weakly hyperfine coupled, phosphorous nuclei, that arise from the two tris(phosphino)borate ligands. The hyperfine splitting of $g_{\perp}$ reveals that at 4K, the odd electron of the formally Fe^{3+} center is fully delocalized over both iron centers. EPR measurements from 77K to 2K show no variation in the measured g values, indicating that the ground state does not localize at low temperature, and that it is isolated from the first excited state. This latter is evidenced by the very small rhombic splitting of $g_{\perp}$ ($\Delta g = g_2 - g_3 = 0.016$) caused by spin-orbit coupling to excited states. As such, **3** is properly considered as a true, $Fe^{2.5+}Fe^{2.5+}$ type-III mixed-valence complex, in the Robin and Day classification scheme for mixed-valence transition metal complexes.[32]

A comparison of the crystal structures for the neutral ($Fe^{2.5+}$, $Fe^{2.5+}$; **3**) and anionic (Fe^{2+},Fe^{2+} **2**) complexes provides insight into the ground state. Table 1 lists selected geometric values for the $P_3Fe(\mu\text{-}H)(\mu\text{-}NH)FeP_3$ core structure, as well as the corresponding values derived from density functional theory geometry optimization performed on both systems. The oxidation of **2** to **3** results in a contraction of r(FeFe) by approximately 0.1 Å, from 2.66 to 2.56 Å. A similar decrease of 0.093 Å in r(FeFe) is predicted from the DFT calculations (2.766 and 2.673 Å, respectively). As noted above, this trend can be attributed to increased Fe-P **π** backbonding in the reduced congener.[31] The DFT-calculated spin densities at the two iron centers are nearly equal ($\rho_{Fe}(1/2) = 0.56/0.59$), as expected for a fully delocalized ground state.[47]

The ENDOR determination of the hyperfine couplings for the three bridging nuclei provides novel insights into the character of the di-iron core of **3**. The small magnitude and negative absolute sign of the ^{14}N spin density on the bridging N(H) suggests that the [Fe-N(H)-Fe] unit behaves analogously to the allyl radical. In a Hückel molecular orbital formulation of the allyl radical, 50% of the unpaired electron is on C(1) and 50% on C(3), with a node at C(2). Incorporation of electron correlation induces spin polarization that leads to a negative spin density on C(2).[48] In **3**, the odd electron is likewise symmetrically delocalized over the two Fe ions, with a small (negative) spin density at the bridging N, consistent with the small spin density found with the DFT computation, $\rho_{DFT}(N) = 0.0155$; given the small net spin density, it is hardly surprising that the experimental and calculated signs do not agree. The analogy between the odd-electron distribution on the Fe-N(H)-Fe center and that on the allyl radical is reminiscent of the recently described analogy between a Fe-N(H)N(H)-Fe center and the butadiene anion, where the SOMO is minimally delocalized onto the central nuclei.[49]

The experiments reveal an isotropic hyperfine coupling for the bridging hydride of a_{iso} = -38.9 MHz; given the coupling for one electron in a ^{1}H 1s orbital, $a_{iso}^{0} = 1420$ MHz,[41] this corresponds to a very small spin density on the hydride, $\rho(^{1}H_{\mu}) = -0.027$.[41] In agreement, the DFT computation likewise yields a small negative spin density on hydride, $\rho_{DFT}(^{1}H_{\mu}) = -0.038$[50] comparable values have been seen in other ENDOR studies of metal-bound hydrides.[3,15]

Recently, a paramagnetic, mixed valence low-spin [Fe^{1+},Fe^{2+}] hydrogenase model complex has been characterized by Jablonskyte, et al.[15] Solution EPR measurements of this complex in THF solution at T = 165 K reveal the presence of a single, hydride with an isotropic hyperfine coupling of a_{iso} = -75.8 MHz. The authors propose that this proton adopts a bridging geometry, but a definitive frozen-solution EPR/ENDOR spectroscopic study or X-ray diffraction characterization is required for confirmation of a bridging, versus a terminal[16] geometry.

Testing the Point-Dipole Calculation of Anisotropic Couplings to Bridging Protons

Turnover of the V70I mutant of the nitrogenase enzyme under an Ar atmosphere followed by rapid freeze quenching generates a new $S = 1/2$ intermediate signal previously unobserved in the wildtype enzyme.[1] A combination of ^{1}H ENDOR spectroscopy[1] and step annealing[11] revealed that this new species represents the E_4 state of the enzyme, in which the FeMo-cofactor has accumulated four electron/proton equivalents.[51] The ^{1}H ENDOR measurements revealed the presence of two strongly hyperfine coupled metal-bound hydrides with equivalent hyperfine tensors, **A**(1) = [11, 25, 37] and **A**(2) = [33, 10, 24] MHz.

The anisotropic component of the hyperfine tensors for the hydrides exhibits a rhombic anisotropic interaction of the form $\mathbf{T} \approx [-t, 0, t]$, t = 10-12 MHz. Application of the point-dipole model for the anisotropic coupling in a [M-H-M] fragment[52] led to the conclusion that these interaction tensors are associated with hydride ions that bridge two metal ions of the cofactor, and that the dipolar interaction arises from the sum of through-space point-dipolar interactions with the exchange-coupled spins of the two anchor metal ions. Subsequently, this point-dipole model was used to conclude that the hydrides bridge two Fe ions, and thus correspond to [Fe-H-Fe] fragments.[1,10]

These conclusions rested on use of the point-dipole interaction model to identify a bridging hydride, and to distinguish such an entity from a terminal hydride. To test this model, we have examined the crystallographically characterized [Fe-H-Fe] fragment of **3**, modeling the through-space dipolar couplings of the bridging hydride and imido proton as the sum of the individual dipolar couplings to symmetrically delocalized spin on the two Fe ions. The point-dipole model precisely reproduces the experimentally derived ^{1,2}H dipolar tensors for **3**, thus validating the use of this model to assign the resolved ^{1,2}H signals from the E_4 intermediate to Fe-Fe bridging, rather than terminal, hydrides.

The description of the anisotropic proton coupling for a proton located between two adjacent Fe ions is possible because there can be no 'local' anisotropic contribution from p-orbital density on a proton, so the coupling is independent of the nature of the Fe-H bonding. On the other hand, the isotropic coupling of a bridging hydride arises from spin density at the proton itself, and thus is a measure of the bonding. The two bridging hydrides of nitrogenase have large isotropic hyperfine couplings, $a_{iso} \approx \pm 24$ MHz. The hyperfine coupling to the bridging hydride in **3** is roughly two-thirds larger, a_{iso} = -38.5 MHz. However, the hydride in **3** bridges a mixed-valence, *low-spin* $Fe^{2.5+}$,$Fe^{2.5+}$ center, whereas the hydrides in nitrogenase are commonly thought to bridge high-spin Fe^{3+} centers. The isotropic coupling to a nucleus that arises from spin density on an ion with spin, S, is proportional to the spin density at that nucleus, $a_{un} = \rho a_o/2S$, where ρ is the proton s-orbital spin density, and a_o is the hyperfine constant for a single ($S = ½$) electron in the 1s orbital of H.[53] For **3**, the calculated hydride spin density is $\rho(^1H_\mu)$ = -0.027 spins (see above). From the measured isotropic hyperfine coupling of the hydrides in E_4, $|a_{obs}|$ = 24 MHz, we can estimate a value for the spin density on each hydride. In the light of the recent ^{95}Mo and ^{57}Fe ENDOR studies of E_4, we consider the hydrides as symmetrically bridging Fe ions with spin projection factors of $K_{Fe1} \sim K_{Fe2} \sim \pm 1/2$.[10,54]. If we further assume that both iron ions are

high-spin ferric ($S = 5/2$), then $|a_{un}| = |a_{obs}| = 24$ MHz, yielding $|\rho(H^-)| \sim 0.09$ for each bridging E_4 hydride. Given the uncertainty in the values of the spin projection factors and the spin states of the anchor Fe atoms, the similarity between a_{un} of the two systems is a surprisingly satisfying complement to the definitive analyses of the anisotropic couplings.

Summary

- The application of 35 GHz EPR and ENDOR spectroscopies has confirmed the description of **3** as an $S = 1/2$ type-III mixed-valence di-iron II/III complex in which the unpaired electron is shared equally between the two iron centers. Compounds exhibiting this electron structure are highly unusual.
- $^{1,2}H$ and $^{14,15}N$ ENDOR measurements of the bridging imide show a very small, negative π spin density arising from polarization by the spin density at iron, consistent with an allyl radical molecular orbital model for the [Fe-(NH)-Fe] fragment.
- Both the bridging hydride and the proton of the bridging (NH) of the crystallographically characterized **3** show the signature of a 'bridging' hydride that is essentially equidistant between two 'anchor metal ions: a rhombic dipolar interaction tensor, $\mathbf{T} \approx [T, -T, 0]$. The point-dipole model for describing the anisotropic interaction of a μ-H^- within an $[M_1\text{-}H^-\text{-}M_2]$ fragment as the sum of the point-dipole couplings to the 'anchor' metal ions reproduces this signature with high accuracy, and the computed tensor smoothly evolves into the signature axial tensor, $\mathbf{T} \approx [T, -T, 2T]$ for a terminal hydride as the proton is moved to one side of the $[M_1, M_2]$ unit, thus validating both the model and the signatures.
- This validation in turn strongly supports the assignment, based on such a point-dipole analysis, that the molybdenum-iron cofactor of nitrogenase contains two [Fe-H-Fe] bridging-hydride fragments in the intermediate state that has accumulated four reducing equivalents (E_4).
- The similarity between the isotropic hyperfine couplings for the bridging hydrides in **3** and E_4 provides a surprisingly satisfying complement to the definitive analyses of the anisotropic couplings.
- This study provides a foundation to the spectroscopic study of hydrides in numerous reducing metalloenzymes, including nitrogenase and the hydrogenases.

Supplementary Material

Refer to Web version on PubMed Central for supplementary material.

Acknowledgments

This work was supported by the NIH (HL13531, BMH; GM070757, JCP). CTS was supported by an NSF Graduate Fellowship. We thank Dr. Peter Doan for helpful conversations, and Mr. Clark Davoust for his invaluable technical expertise.

References

1. Igarashi RY, Laryukhin M, Santos PCD, Lee H-I, Dean DR, Seefeldt LC, Hoffman BM. J Am Chem Soc. 2005; 127:6231. [PubMed: 15853328]
2. Fan C, Teixeira M, Moura J, Moura I, Huynh B-H, le Gall J, Peck HD Jr, Hoffman BM. J Am Chem Soc. 1991; 113:20.
3. Stein M, Lubitz W. Phys Chem Chem Phys. 2001; 3:5115.
4. Lubitz W, Reijerse E, van Gastel M. Chem Rev (Washington, DC, U S). 2007; 107:4331.

5. Amara P, Mouesca J-M, Volbeda A, Fontecilla-Camps JC. Inorg Chem (Washington, DC, U S). 2011; 50:1868.
6. Harmer J, Finazzo C, Piskorski R, Ebner S, Duin EC, Goenrich M, Thauer RK, Reiher M, Schweiger A, Hinderberger D, Jaun B. J Am Chem Soc. 2008; 130:10907. [PubMed: 18652465]
7. Yandulov DV, Schrock RR. Science (Washington, DC, U S). 2003; 301:76.
8. Lukoyanov D, Dikanov SA, Yang Z-Y, Barney BM, Samoilova RI, Narasimhulu KV, Dean DR, Seefeldt LC, Hoffman BM. J Am Chem Soc. 2011; 133:1655.
9. Hoffman BM, Dean DR, Seefeldt LC. Acc Chem Res. 2009; 42:609. [PubMed: 19267458]
10. Lukoyanov D, Yang Z-Y, Dean DR, Seefeldt LC, Hoffman BM. J Am Chem Soc. 2010; 132:2526. [PubMed: 20121157]
11. Lukoyanov D, Barney BM, Dean DR, Seefeldt LC, Hoffman BM. Proc Natl Acad Sci U S A. 2007; 104:1451. [PubMed: 17251348]
12. Thorneley R, Lowe D. Biochem J. 1984; 224:887. [PubMed: 6395862]
13. Siegbahn PEM, Tye JW, Hall MB. Chem Rev (Washington, DC, U S). 2007; 107:4414.
14. Jablonskyte A, Wright JA, Pickett CJ. Dalton Trans. 2010; 39:3026–3034. [PubMed: 20221536]
15. Jablonskytė A, Wright JA, Fairhurst SA, Peck JNT, Ibrahim SK, Oganesyan VS, Pickett CJ. J Am Chem Soc. 2011; 133:18606. [PubMed: 22035325]
16. Kinney RA, Hetterscheid DGH, Hanna BS, Schrock RR, Hoffman BM. Inorg Chem (Washington, DC, U S). 2010; 49:704.
17. Chiang K, Scarborough C, Horitani M, Lees N, Ding K, Dugan T, Brennessel W, Bill E, Hoffman B, Holland P. Angew Chem Int Ed. 2012; 51:1.
18. Brown SD, Mehn MP, Peters JC. J Am Chem Soc. 2005; 127:13146. [PubMed: 16173733]
19. Sheldrick GM. Acta Crystallogr, Sect: A Found Crystallogr. 1990; A46:467.
20. Sheldrick GM. Acta Crystallogr, Sect A: Found Crystallogr. 2008; A64:112.
21. Mueller, P.; Herbst-Irmer, R.; Spek, AL.; Schneider, TR.; Sawaya, MR. Crystal Structure Refinement: A Crystallographer's Guide to SHELXL. Oxford University Press; Oxford: 2006.
22. Werst MM, Davoust CE, Hoffman BM. J Am Chem Soc. 1991; 113:1533.
23. Davoust CE, Doan PE, Hoffman BM. J Magn Reson. 1996; 119:38.
24. Zipse H, Artin E, Wnuk S, Lohman GJS, Martino D, Griffin RG, Kacprzak S, Kaupp M, Hoffman B, Bennati M, Stubbe J, Lees N. J Am Chem Soc. 2009; 131:200. [PubMed: 19128178]
25. Hoffman BM, DeRose VJ, Ong JL, Davoust CE. J Magn Reson. 1994; 110:52.
26. Lee H-I, Igarashi RY, Laryukhin M, Doan PE, Dos Santos PC, Dean DR, Seefeldt LC, Hoffman BM. J Am Chem Soc. 2004; 126:9563. [PubMed: 15291559]
27. Hoffman BM. Acc Chem Res. 1991; 24:164.
28. Doan, PE. Paramagnetic Resonance of Metallobiomolecules. Telser, J., editor. American Chemical Society; 2003. p. 55
29. Doan PE. J Magn Reson. 2011; 208:76. [PubMed: 21075026]
30. ADF 2010.01, SCM, Theoretical Chemistry. Vrije Universiteit; Amsterdam, The Netherlands: http://www.scm.com
31. Brown SD, Peters JC. J Am Chem Soc. 2005; 127:1913. [PubMed: 15701026]
32. Schatz, P. Inorganic Electronic Structure and Spectroscopy. Lever, ABP.; Solomon, EI., editors. Vol. II. John Wiley & Sons; New York: 1999.
33. Hoffman BM, DeRose VJ, Doan PE, Gurbiel RJ, Houseman ALP, Telser J. J Biol Magn Reson, (EMR of Paramagnetic Molecules). 1993; 13:151.
34. Hoffman, BM.; Gurbiel, RJ.; Werst, MM.; Sivaraja, M. Advanced EPR Applications in Biology and Biochem. Hoff, AJ., editor. Elsevier; Amsterdam: 1989. p. 541
35. Lee H-I, Dexter AF, Fann Y-C, Lakner FJ, Hager LP, Hoffman BM. J Am Chem Soc. 1997; 119:4059.
36. Hutchison CA Jr, McKay DB. J Chem Phys. 1977; 66:3311.
37. Willems J-P, Lee H-I, Burdi D, Doan PE, Stubbe J, Hoffman BM. J Am Chem Soc. 1997; 119:9816.

38. If we swap g_x and g_y, we obtain $\mathbf{T}'$ = [2.55, −18.9, 16.4] MHz, which leads to an identical conclusion regarding the orientation of **g**
39. Epel B, Manikandan P, Kroneck PMH, Goldfarb D. Appl Magn Reson. 2001; 21:287.
40. Epel B, Poppl A, Manikandan P, Vega S, Goldfarb D. J Magn Reson. 2001; 148:388. [PubMed: 11237646]
41. Weil, JA.; Bolton, JR.; Wertz, JE. Electron Paramagnetic Resonance: Elementary Theory and Applications. John Wiley & Sons; New York: 1994.
42. Yang T-C, McNaughton RL, Clay MD, Jenney Francis E J, Krishnan R, Kurtz Donald M J, Adams MWW, Johnson MK, Hoffman BM. J Am Chem Soc. 2006; 128:16566. [PubMed: 17177406]
43. Scholes CP, Lapidot A, Mascarenhas R, Inubushi T, Isaacson RA, Feher G. J Am Chem Soc. 1982; 104:2724.
44. Lucken, EAC. Nuclear Quadrupole Coupling Constants. Academic Press; New York: 1969.
45. Ammeter JH. J Magn Reson. 1978; 30:299.
46. McNaughton RL, Roemelt M, Chin JM, Schrock RR, Neese F, Hoffman BM. J Am Chem Soc. 2010; 132:8645. [PubMed: 20429559]
47. Single-point calculations on the optimized geometry of **4** (BLYP functional) that utilize the hybrid B3LYP density functional predict a localization of the iron valency (ρ_{Fe} = -0.0143, 1.2783), in contrast to experimental evidence.
48. Carrington, A.; McLachlan, AD. Introduction to magnetic resonance with applications to chemistry and chemical physics. Harper & Row; New York: 1967.
49. Saouma CT, Kinney RA, Hoffman BM, Peters JC. Angew Chem Int Ed. 2011; 50:3446.
50. The increased magnitude of the hydride spin density is consistent with DFT overestimating the influence of spin polarization. See Radon M, et al. J Phys Chem B. 2010; 114:1518–1528. [PubMed: 20047294]
51. Thorneley RN, Lowe DJ. Biochem J. 1983; 215:393. [PubMed: 6316927]
52. DeRose VJ, Liu KE, Lippard SJ, Hoffman BM. J Am Chem Soc. 1996; 118:121.
53. Atherton, NM. Principles of Electron Spin Resonance. Ellis Horwood; New York: 1993.
54. Doan PE, Telser J, Barney BM, Igarashi RY, Dean DR, Seefeldt LC, Hoffman BM. J Am Chem Soc. 2011; 133:17329. [PubMed: 21980917]

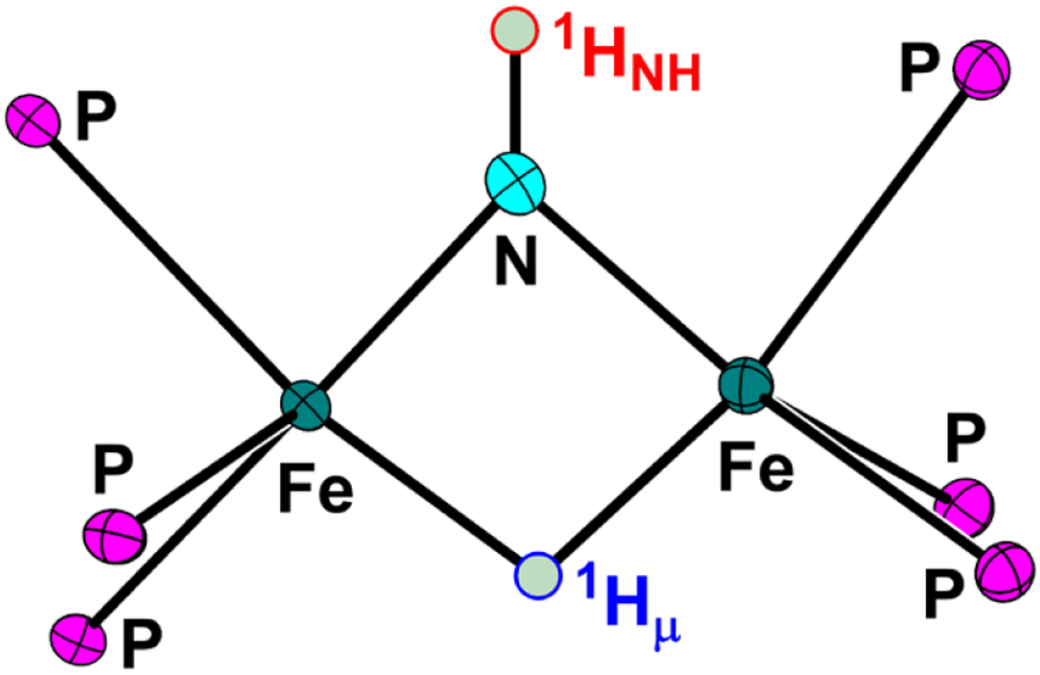

Figure 1.
Thermal ellipsoid (50 %) representation of the core atoms of mixed-valence **3**.

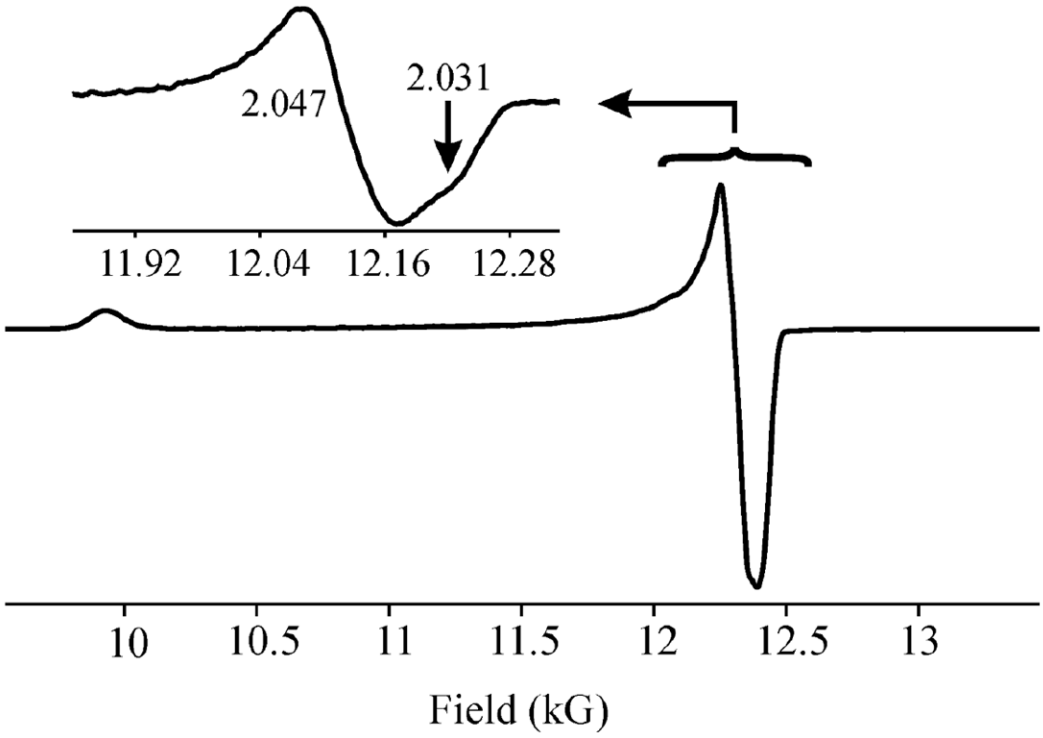

Figure 2.

35 GHz EPR spectrum of **3**. *Main:* Numerical derivative of the CW absorption-display spectrum. *Inset* The small rhombic splitting ($\Delta(g_2\text{-}g_3) = 0.016$ (101 G)) of the perpendicular region of the spectrum (inset). *Experimental conditions*: T = 2 K; modulation amplitude, 0.33 G; microwave power, 0.01 mW; microwave frequency, 35.300 GHz. *Inset*: Davies pulse sequence, $\pi = 80$ ns; $\tau = 600$ ns; repetition time, 20 ms; scan time, 200 s; microwave frequency, 34.714 GHz.

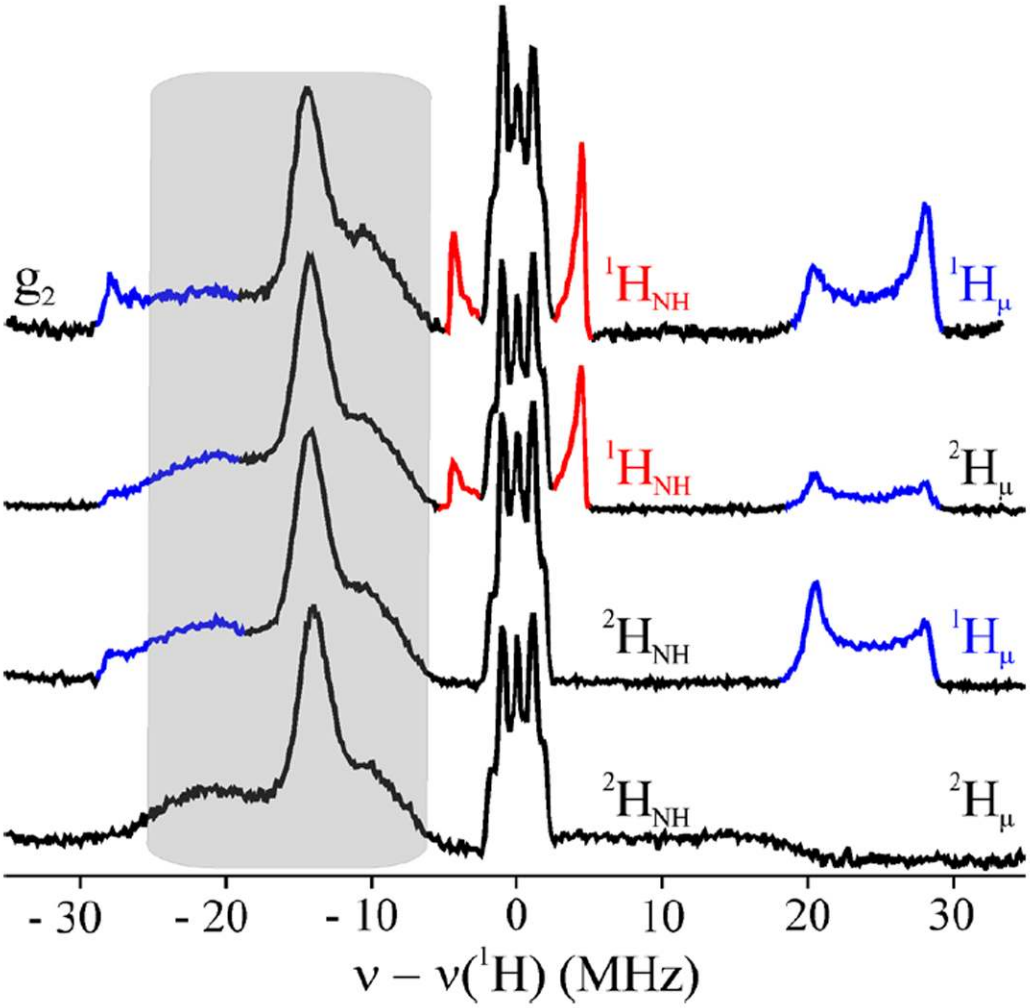

Figure 3.

^{1}H ENDOR spectra measured at g_2 = 2.047 for the complexes (top to bottom): $[Fe]_2$(H)(NH), $[Fe]_2$(D)(NH), $[Fe]_2$(H)(ND), $[Fe]_2$(D)(ND). All compounds are 2 mM in 1:9 2-methyl THF:THF. Spectral intensities are normalized to the intensity of the ^{31}P ENDOR response at -12 MHz. The ENDOR response from the hydride ligand and the imido ligand proton are marked in blue and red, respectively. The ^{31}P ENDOR response is marked by the gray box. *Experimental conditions*: microwave frequency, 34.984 to 35.342 GHz; modulation amplitude, 1.33 G; RF power, 10 W; microwave power, 100 mW; stochastic CW timings: sample, 1 ms; delay, 1 ms; RF, 0.75 ms; and the bandwidth of RF excitation was broadened to 100 kHz.

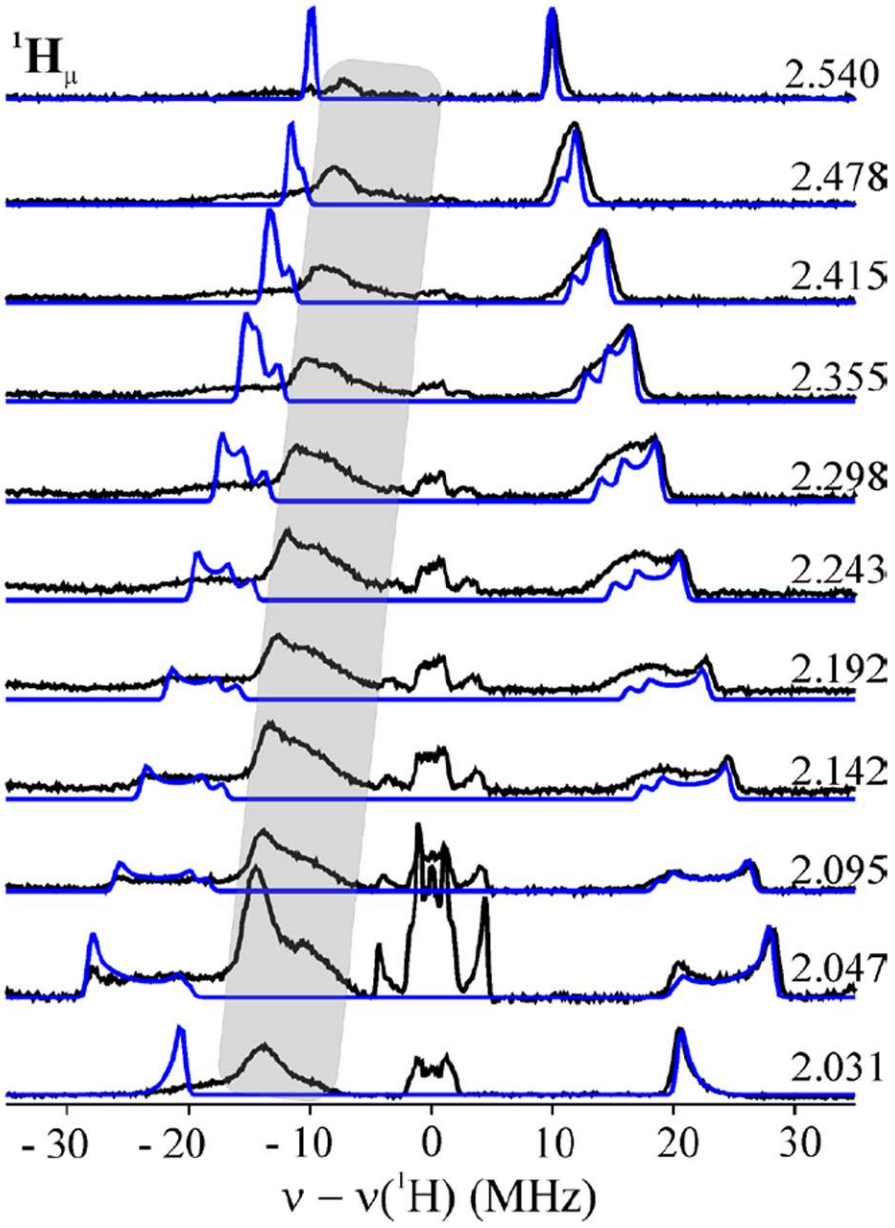

Figure 4.

Stochastic-field modulation-detected ^{1}H ENDOR field-frequency pattern of **3**. Spectra (black) and simulations (blue) are centered at the proton larmor frequency. Spectral intensity is adjusted arbitrarily for clarity. Simulation intensity is normalized to high frequency edge of individual spectra. *Experimental conditions*: microwave power, 10 mW; modulation amplitude, 1.3 G; stochastic sequence timings: sample time, 1 ms; delay time, 1 ms; and RF length, 0.75 ms; time constant, 0 ms; RF power, 10 W; temperature, 2K; and the bandwidth of RF excitation was broadened to 100 kHz. *Simulations*: **g** = [2.54, 2.047, 2.031]; **A** = [19.5, 56.3, 41.0] MHz; (α, β, γ) = (0, 5, 0); EPR linewidth 150 MHz; ENDOR linewidth 0.5 MHz; microwave frequency 35.342 GHz.

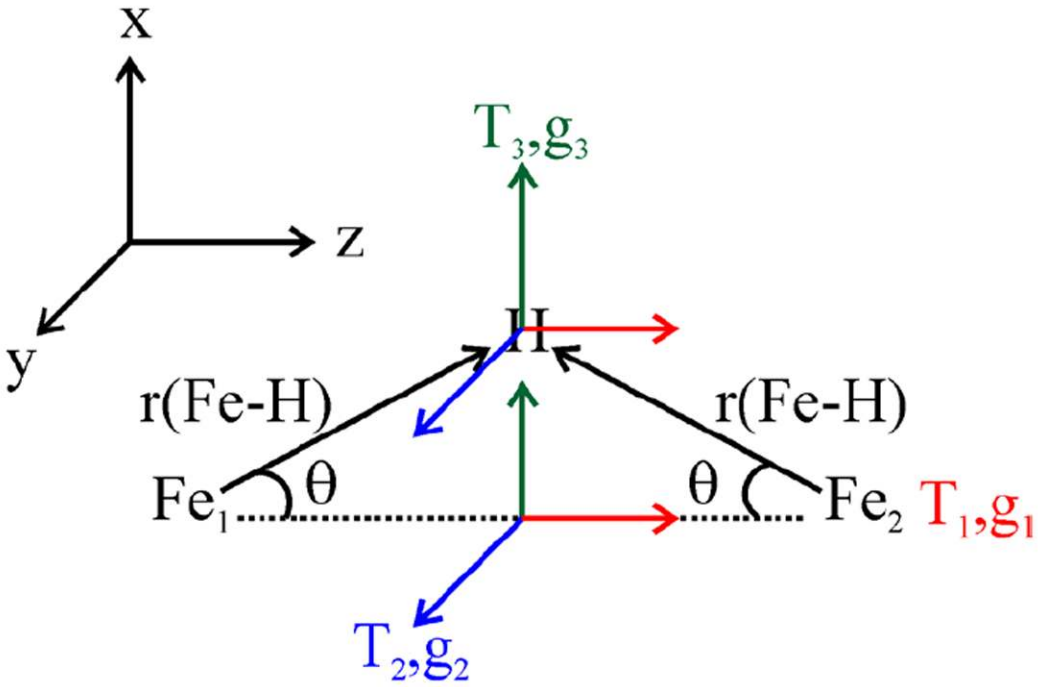

Figure 5.

Schematic representation of the orientation of the g-tensor frame and the hydride dipolar (T) frame within the molecular coordinate system. (l_x^N,l_y^N,l_z^N) (N = 1, 2) are the directional cosines projecting the external magnetic field vector onto the Fe-H bond vectors. Fitting of the experimentally determined principle values of the dipolar tensor yields θ = 38° (the crystal structure value is 40°).

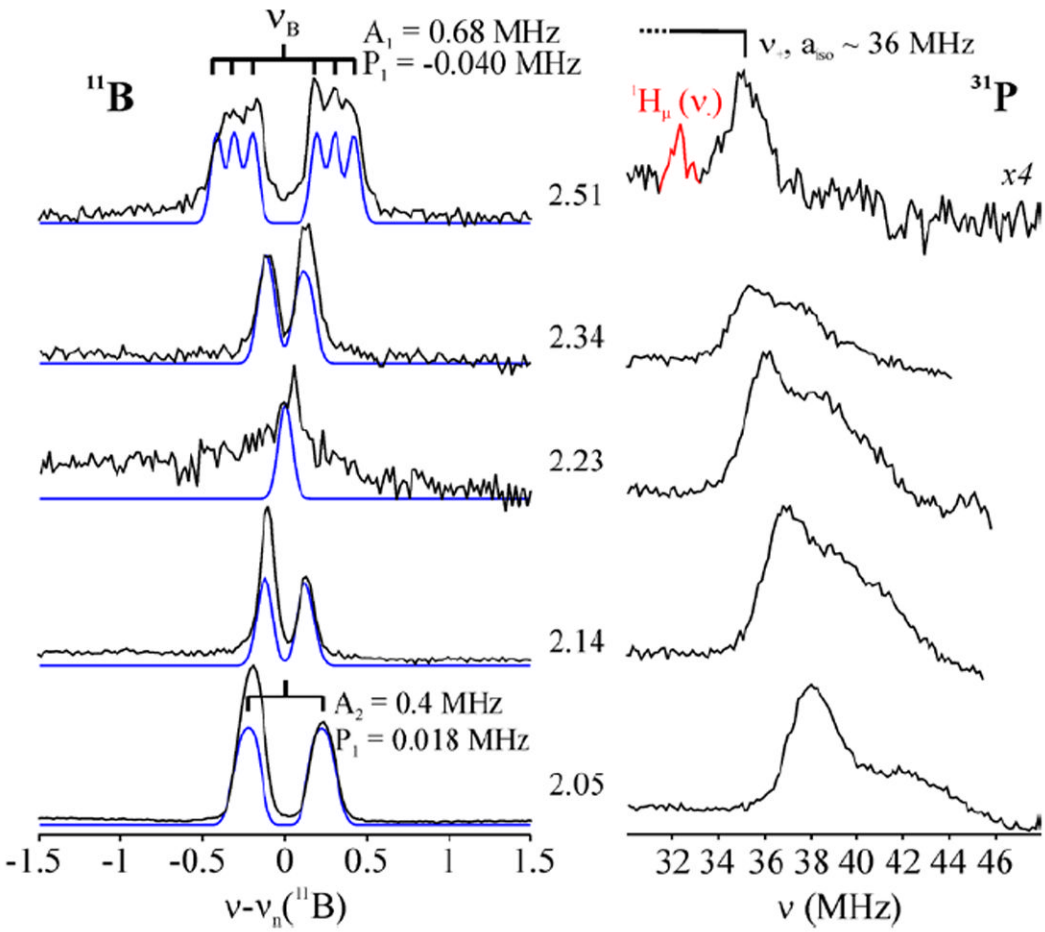

Figure 6.

Field-frequency patterns for ^{11}B (left) and ^{31}P (right) ENDOR of **3**. Simulations of the ^{11}B pattern (blue) employ the hyperfine and quadrupole tensors given in the text. *Experimental Conditions* (^{11}B): Mims pulse sequence, π = 50 ns; stochastic data acquisition; τ = 500 ns; repetition time, 20 ms; t_{RF}, 15 ms; and the RF amplifier output filtered with 20 MHz low pass filter. *Experimental conditions* (^{31}P): microwave power, 10 mW; modulation amplitude, 1.3 G p-p; stochastic sequence timings: sample time, 1 ms; delay time, 1 ms; and RF length, 0.75 ms; time constant, 0 ms; RF power, 10 W; temperature, 2K; and the bandwidth of RF excitation was broadened to 100 kHz.

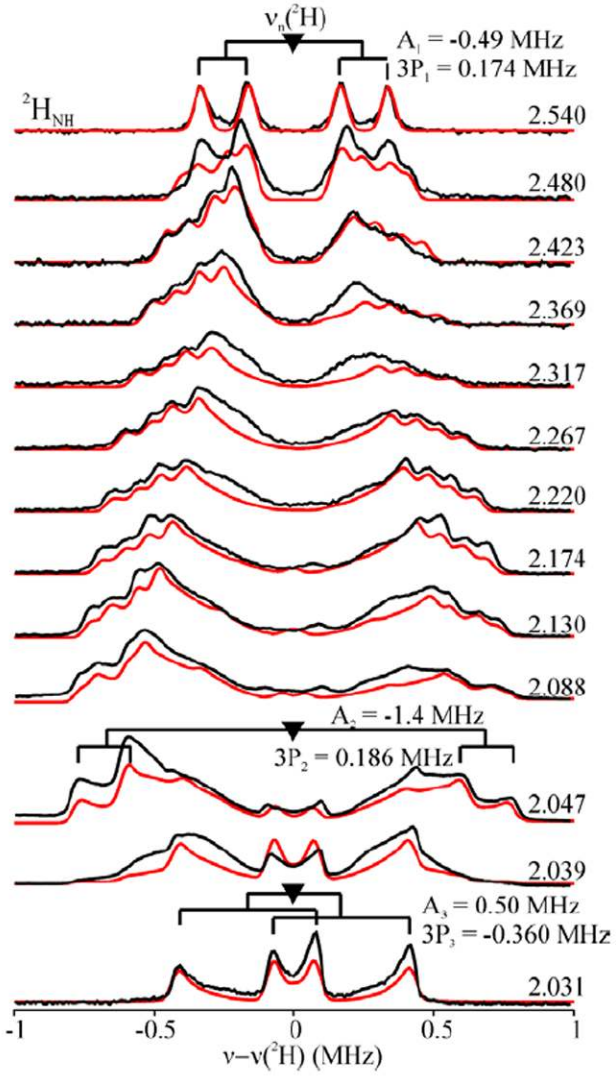

Figure 7.

^2H Mims field-frequency ENDOR pattern from fully-deuterated **3**. The center ($\delta\nu$ = 0 MHz) of the simulated ENDOR pattern was adjusted by +16 G to accommodate an offset in the center field. The simulation intensity was matched to the individual ENDOR spectra for clarity. *Experimental conditions*. Microwave frequency, 34.718 GHz; $\pi/2$ = 50 ns; τ = 500 ns; t_{RF}= 30 μs; repetition rate, 20 ms; RF randomly hopped. *Simulations*. **g** = [2.54, 2.047, 2.031]; **A** = [-0.49, -1.4, 0.5] MHz, (α, β, γ) = (90, 6, 100); **P** = [0.058, 0.062, -0.12] MHz (coaxial) (g_1= z); EPR/ENDOR linewidth = 200/0.05 MHz; τ = 500 ns.

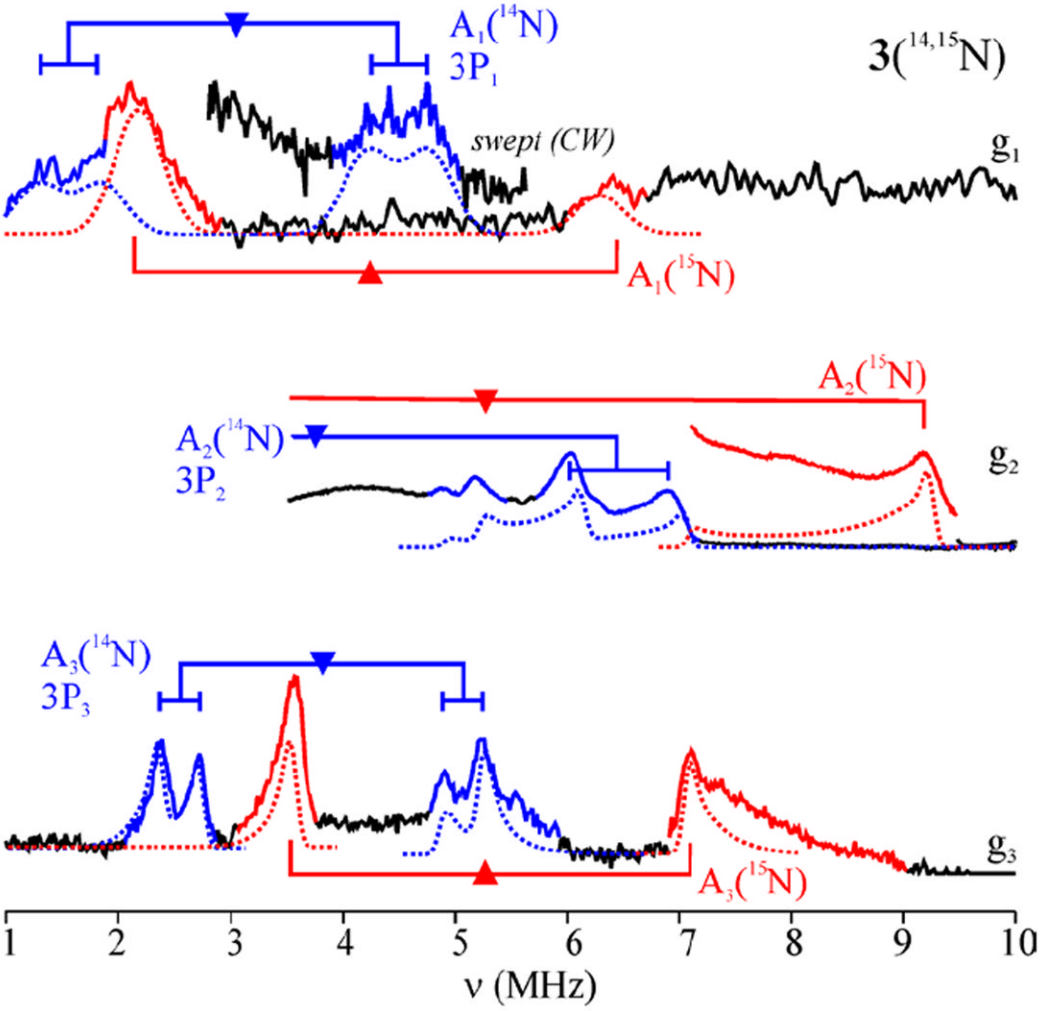

Figure 8.

35 GHz pulse ^{14,15}N Davies ENDOR of **3**(^{14,15}N) measured at the principal g values. The ENDOR responses for the ^{14}N nucleus (blue, solid) and ^{15}N nucleus (red, solid) are noted, with simulations for both (dotted). The inset shows the 35 GHz field-swept ^{14}N ν_+ CW ENDOR response from **3**. *Experimental conditions*: microwave frequency, 34.934 GHz; π = 200 ns; τ = 600 ns; t_{rf} = 30 μs, repetition rate, 20 ms; and the RF was hopped randomly. *Inset*: microwave frequency, 35.326 GHz, microwave power, 0.01 mW; modulation amplitude, 0.33 G; temperature, 2K. *Simulations*: g = [2.54, 2.047, 2.031]; ^{14}N: **A** = -[3, 5.7, 2.5] MHz, **P** = [0.19, -0.31, 0.12] MHz; ^{15}N: **A** = +[4.1, 8, 3.5] MHz; **A** and **g** (and **P** for ^{14}N) are coaxial.

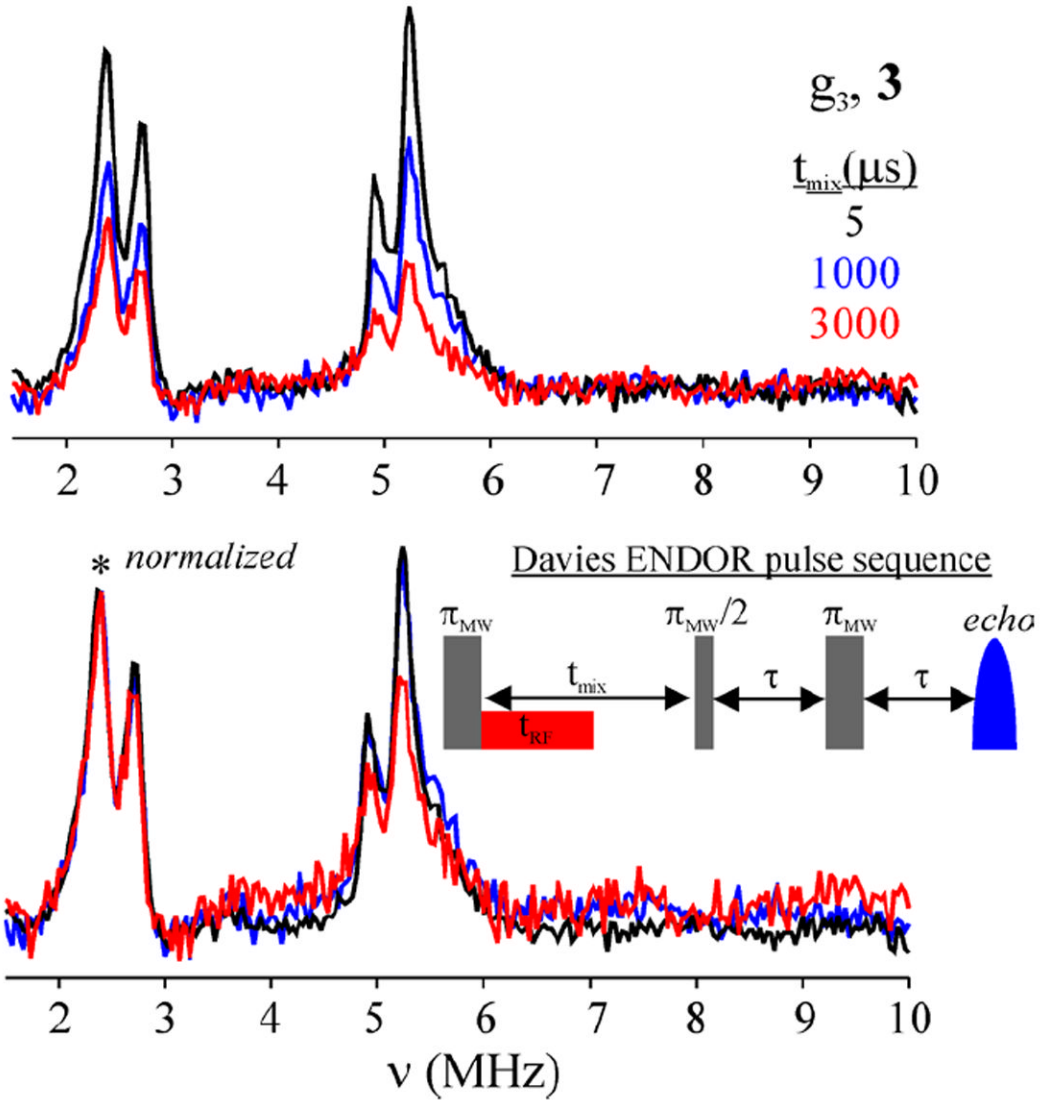

Figure 9.

Variable mixing time ^{14}N Davies ENDOR of **3** at g_3= 2.031. The spectra shown have been displayed as a direct overlay (*top*) and as normalized at $\nu_-(^{14}N; *)$ (*bottom*). *Experimental conditions*. Microwave frequency, 34.986 GHz; repetition rate, 20-23 ms; τ = 600 ns; RF randomly hopped.

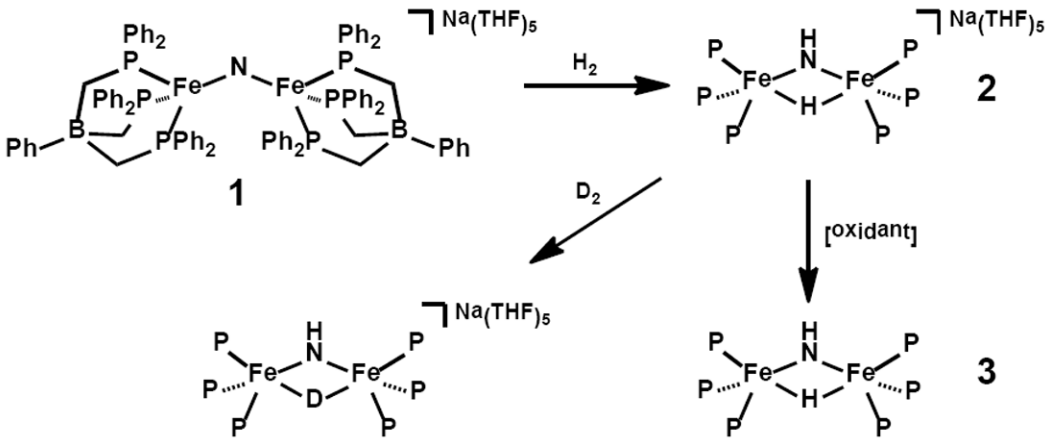

Scheme 1.

Table 1

Table of selected bond lengths for **2** and **3** as obtained from x-ray crystallography (xtal) and from DFT geometry optimization.

	2(Xtal)	2(DFT)	3(Xtal)	3(DFT)
Fe_1H	1.51(2)	1.775	1.68(3)	1.731
Fe_2H	1.51(2)	1.754	1.64(3)	1.734
Fe_1N	1.826(5)	1.808	1.777(3)	1.805
Fe_2N	1.790(5)	1.807	1.783(3)	1.796
Fe_1P_1	2.2024(13)	2.323	2.2539(8)	2.382
Fe_1P_2	2.2121(13)	2.397	2.2975(8)	2.413
Fe_1P_3	2.2274(13)	2.291	2.3027(8)	2.391
Fe_2P_1	2.2247(13)	2.345	2.2799(8)	2.359
Fe_2P_2	2.2306(13)	2.400	2.2930(8)	2.435
Fe_2P_3	2.2411(13)	2.337	2.3151(8)	2.466
NH	0.879(7)	1.023	0.89(2)	1.025
Fe_1Fe_2	2.6595(9)	2.766	2.5596(6)	2.673

All values give are in angstroms. [18] The NH/H positions are disordered in the solid-state structure of **2**, and only the bond distances to the major component of the disorder are given.